Control of the microstructure and mechanical properties of electrodeposited graphene/Ni composite

Yongsheng Liu, Ying Liu, Qian Zhang, Caili Zhang, Jian Wang, Yanxia Wu, Peide Han, Zhipeng Gao, Liping Wang, Xiaolei Wu

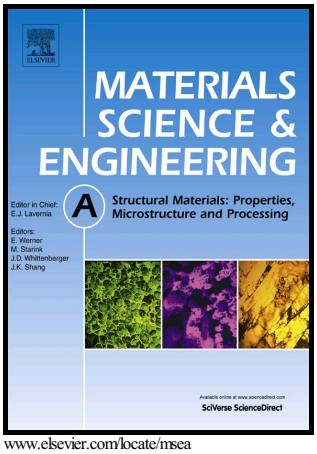

www.elsevier.com/locate/msea

PII: S0921-5093(18)30598-7
DOI: https://doi.org/10.1016/j.msea.2018.04.092
Reference: MSA36412

To appear in: *Materials Science & Engineering A*

Received date: 2 March 2018
Revised date: 11 April 2018
Accepted date: 21 April 2018

Cite this article as: Yongsheng Liu, Ying Liu, Qian Zhang, Caili Zhang, Jian Wang, Yanxia Wu, Peide Han, Zhipeng Gao, Liping Wang and Xiaolei Wu, Control of the microstructure and mechanical properties of electrodeposited graphene/Ni composite, *Materials Science & Engineering A*, https://doi.org/10.1016/j.msea.2018.04.092

Control of the microstructure and mechanical properties of electrodeposited graphene/Ni composite

Yongsheng Liu[a], Ying Liu[a*], Qian Zhang[a], Caili Zhang[a], Jian Wang[a], Yanxia Wu[a], Peide Han[a,b*], Zhipeng Gao[c], Liping Wang[a], Xiaolei Wu[d]

[a]College of Materials Science and Engineering, Taiyuan University of Technology, Taiyuan 030024, PR China.

[b]Key Laboratory of Interface Science and Engineering in Advanced Materials, Taiyuan University of Technology, Taiyuan 030024, PR China.

[c]Institute of Applied Mechanics & Biomedical Engineering, College of Mechanics, Taiyuan University of Technology, Taiyuan 030024, PR China.

[d]State Key Laboratory of Nonlinear Mechanics, Institute of Mechanics, Chinese Academy of Sciences, Beijing 100190, PR China

liuying01@tyut.edu.cn

hanpeide@126.com

[*]Corresponding authors. Tel.: 86-351-6014218.

Abstract

Nickel composites reinforced with reduced graphene oxide (rGO) nanosheets were fabricated by a direct current electrodeposition technique. The low volume fraction of graphene can promote the cathodic polarized potential, facilitate the transport of ions and electrons on electrodes, and provide a large number of nucleation sites, consequently accelerate the formation of heterogeneous microstructure features. The graphene/Ni composite with 2 mL graphene dispersions demonstrates a tensile strength of 864 MPa and a plastic elongation of 20.6 %, which are 25 % and 36 % higher than that of the pure bulk Ni. The enhancements in strength and ductility of the composite can be ascribed to the bimodal microstructure, for which the fine grain population provides for enhanced strength, whereas the coarse grain population enhances ductility by enabling strain hardening. On the contrary, the positive role of rGO in microstructure control will be weakened due to the agglomeration of rGO sheets in a high-volume plating bath. The low adsorption quantity of rGO is unfavourable for the nucleation of Ni matrix, accordingly produces a uniform fine-grained microstructure. The tensile strength of the composite with 5 mL rGO is 750 MPa, whereas the fracture elongation is only 7.5 %. It is believed that a proper addition of rGO dispersion makes a promising microstructure for advanced graphene/Ni composite.

Keywords: graphene/Ni composites, electrochemical nucleation, heterogeneous microstructure, strength and ductility

1. Introduction

Graphene, a two-dimensional building block of carbon material with a single atomic layer of sp^2 hybridized carbon atoms densely packed in a honeycomb lattice, has a great potential as an ideal strength enhancer in metal matrix composites owing to its special structural characteristic and excellent mechanical properties [1]. Previous reports show that the elastic modulus, yield strength, and electrical conductivity of metal matrix composites can be significantly enhanced even though a low volume fraction of graphene is added [2,3]. However, the main obstacles for obtaining excellent reinforcement efficiency in graphene reinforced metal composites are the agglomeration between graphene nanosheets in manufacturing process, and the poor affinity of graphene with metal matrix [4,5]. On the other hand, most of the graphene/metal composites are prepared by mechanical alloying and metallurgy method [6-8]. During the high energy ball milling and high temperature metallurgy process, graphene nanosheets will be damaged, thus results in degraded strengthening ability of graphene on the composites [9-11]. Therefore, it is still necessary to develop a high efficiency, easy operation and low temperature fabrication method for graphene/metal composites, which can achieve a homogeneous dispersion of the reinforcement, robust the interface, as well as reduce the damage of the graphene structure.

Electrodeposition is one of the most efficient methods for fabricating metal materials due to its simple and stable process, which has special advantages in the microstructure and property modifications of the depositions. By adjusting the electrodeposition parameters, such as the deposition potential, current densities, electrolyte composition, PH value, temperature, etc., the components, phases, and microstructures of the deposits can be controlled [12]. Specially, a variety of nonuniform architectures, including the lamella structure [13], gradient structure [14], bimodal structure [15], as well as trimodal structure [16], which are more favourable to take full advantage of the coupling effect among the constituent phases, have been prepared by precisely controlling the nucleation and growth processes of the deposits. Thus, electrodeposition is a good choice to synthesis graphene reinforced metal matrix composites that can achieve high yield strength and good uniform tensile elongation.

Recently, graphene reinforced nickel matrix composites (graphene/Ni composites) with specific mechanical properties have been synthesized by electrodeposition approach. Kuang et al. prepared the graphene/nickel composites by the co-electrodeposition of Ni ions and graphene oxide (GO) sheets. The composite with 0.12 wt% has a hardness of 6.85 GPa and an elastic modulus of 252.76 GPa, for which the hardness increases almost 4-fold compared to the pure Ni electrodeposits [17]. Li et al. developed a pulse-reverse electrodeposition method to fabricate graphene/Ni composite with high graphene content, and found

the crystalline refinement strengthening and possible pinning effect rendered by graphene to hinder dislocation at interface. The composite exhibits 2.7-fold enhancement of Vickers hardness, while the Young's modulus quantifies 1.4-fold increasing [18]. Nevertheless, to the best of our knowledge, GO sheets rather than graphene nanoflakes have been used as the source reinforcements in the plating baths. The GO show good dissolvability in water and can be reduced in electroplating process, but it will become instability in plating solution due to the existing hydroxyl and carboxyl groups on surfaces [19,20]. The organic functional groups can absorb a large number of metal cations after hydrolysis reaction, inducing the decrease in Zeta potential of GO dispersions. As a result, the stable disperse state of the GO colloids will be changed, the quality control of graphene/Ni composite is much more difficult and complicated in the GO contained plating baths. In contrast, if graphene dispersions are used, it not only can bring out the uniformly dispersing graphene nanosheets in nickel matrix, but also the complete structural graphene can keep its high strength enhancing efficiency. Both the strength and ductility of the electrodeposited graphene/Ni composites are expected to be further improved.

On the other hand, differ from the commonly used second-phase reinforcements [21], such as carbon nanotubes, SiC, Al_2O_3, SiO_2 nanoparticles, and so on, graphene with high aspect ratio and large surface area can observably influence the electro-crystallization nucleation and growth processes of metal matrix. Ren et al

revealed that the incorporation of graphene in the nickel matrix could increase both the inter-planar spacing and the degree of preferred orientation of crystalline nickel [22]. Wang et al. found that the GO in GO/Ni foils not only effectively lowered the matrix grain size but also contributed to the growth of Ni toward the (111) direction [23]. However, Pavithra et al. [24] and Li et al. [25] proposed that the addition of GO could not influence the deposit formation of Ni and did not change the plane of the preferred orientation, but accelerated the formation of nuclei, inhibited the growth of grain and improved the crystallinity. What's the inherent mechanisms on the microstructural evolution of graphene/Ni composites formed in electroplating process? How do the concentration, size, and distribution of graphene influence the microstructures and mechanical properties of electrodeposited graphene/Ni composites? All these problems are still need further investigation.

In this work, by using the dispersible reduced graphene oxide (rGO) as the reinforcement in the plating solution, graphene/Ni composites which exhibit high strength and good ductility have been synthesized. The influence of graphene contents on the microstructural formation and mechanical properties of the graphene/Ni composites have been fully investigated. The strengthening and toughing mechanism of the as-synthesized graphene/Ni composites are rationally discussed as well.

2. Experimental

2.1 Preparation of the reduced graphene oxide

All the reagents were analytical grade and used without further purification. The GO dispersion (2 mg/mL in water) was provided by Institute of Coal Chemistry, Chinese Academy of Sciences. In the typical synthesis procedure of the dispersible rGO, 5 mL GO dispersion was added to a solution containing 20 mg polyvinyl pyrrolidone (PVP), 30 mL distilled water, 4 mL NaOH (1 mol/L), and 1 mL $N_2H_4 \cdot H_2O$. The mixture was kept at 80 °C for about 5 h with ultra-sonication. Then, the solution was filtered by dialysis membrane (MD34-5M) to remove residual PVP molecules. After a filtration process for 5 days, the homogeneous rGO solution was obtained.

2.2 Fabrication of the graphene/Ni composites

The 304 stainless steel substrate (50 mm in length, 40 mm in width, and 1 mm in thickness) and Ni plate (purity quotient of 99.9 %) were used as the cathode and anode, respectively. The area ratio between the anode and cathode is 3:2. Before depositing, the 304 stainless steel plates were ultrasonic cleaned in acetone and ethyl alcohol, respectively. Then, they were immersed in a 0.01 mol/L HCl solution to remove the oxide layer and washed with deionized water.

The electroplating bath consisted of 250 g/L $NiSO_4 \cdot 6H_2O$, 35 g/L $NiCl_2 \cdot 6H_2O$, 35g/L H_3BO_3 and 40 mg/L sodium dodecyl benzene sulfonate, was used to produce the samples at 55 °C. The electrolyte was strictly purified for two days under a low current density of 0.4 A/dm^2 for 24 h before the electrodeposition.

During the electroplating process, the PH value of the electrolyte is maintained at 4.37 by a 0.01 mol/L HCl solution. The pure Ni foil with a thickness of about 300μm was obtained after direct current electrodeposition with a current density of 3.5 A/dm^2 for 12 h. In addition, graphene/Ni composites with different components and microstructures were fabricated by adding the as-synthesized rGO dispersion (1 mL, 2 mL, 3 mL, 4 mL and 5 mL, respectively) into the bath.

2.3 Characterization and measurements

The Raman scattering was performed on a Raman spectrometer (X-PLORA) using a 532 nm laser source, while the FT-IR spectra were investigated on a FT-IR spectrometer (TENSOR27) over a range from 400 to 4000 cm^{-1}. The morphology and microstructure of the rGO nanoflakes were characterized by a scanning electron microscopy (NovaNanoSEM430) and a transmission electron microscopy (JEM-2100, acceleration voltage of 200 kV), respectively. Crystallographic orientations of the samples were measured by a Rigaku D/max-2500PC with Cu Kαradiation. The chemical compositions of the products have been characterized by the Carbon/Sulfur Analyzer (EMIA 832). By cutting the materials into dog-bone-shaped samples with a gauge length of 14 mm and width of 2.5 mm, the mechanical properties of the composites were tested on an Instron 5544 testing machine at the strain rate of $1.19\times10^{-3}\ s^{-1}$. The microstructures of specimens were characterized by the electron back scatter diffraction (EBSD, TSL OIM system on the Philips XL30 FEG SEM) with step sizes of 250 nm, while the

electro-crystallization behaviours of the graphene/Ni composites were performed on a CS350H electrochemical workstation (Wuhan Corrtest Instruments Corp. Ltd., China) at 55 °C. In order to ensure the consistency of all experimental conditions, the electroplating baths with different graphene contents, 304 stainless steel substrates, Ni plates, and a saturated calomel electrode (SCE) were used as the electrolyte, the counter electrode, the working electrode, and the reference electrode, respectively. The cyclic voltammograms (CV) were measured at a scan rate of 10 mV/s, while the electrochemical impedance spectra (EIS) were tested in the signal amplitude of 20 mV with a frequency range from 10^{-2} Hz to 10^{5} Hz.

3. Results and discussion

Fig.1A shows the Raman spectra of graphene oxide and reduced graphene oxide, respectively. The Raman vibration characteristics of rGO are similar to that of the GO. The Raman spectrum of GO displays a strong G band at 1583 cm^{-1}, a slightly weak D band at 1352 cm^{-1}, and a broad 2D band at 2691 cm^{-1}, which are arose from the in-plane bond-stretching motion (the E_{2g} phonons) of the pairs of C sp^2 atoms, the breathing modes of rings or K-point phonons of A_{1g} symmetry, and the double-resonant scattering of electrons and holes from phonons between states located on the Dirac cones at the K points, respectively [26]. In contrast, due to the reduction of functional groups can generate on the electronic structure of the C network and thereby hamper the resonant Raman processes [27], the G band of rGO shifts upward to 1594 cm^{-1}, while the D band turns to line at 1340 cm^{-1}. On

the other hand, the intensity ratio between the D and G band of the samples has changed. The intensity ratio (I_D/I_G) of GO and rGO are 0.92 and 1.05, respectively, which is in line with Guo's results [28]. According to the above analysis, it can be seen that rGO was synthesized.

To further understanding the quality of rGO, FTIR spectra are used to analyze the functional groups. Fig. 1B shows the FTIR spectra of the GO and rGO. The spectrum of GO exhibits four characteristic peaks at 3421 cm^{-1}, 1619 cm^{-1}, 1368 cm^{-1}, and 1163 cm^{-1}, which are corresponded to the hydroxyl, benzene ring, carboxyl, and epoxy groups, respectively [29,30]. This means that there are abundant oxygen-containing functional groups on the surface of GO. However, as for the rGO, the intensity of O-H stretching characteristic peak at 3421 cm^{-1} becomes weaker, namely a large number of O-H groups have been removed. Whereas the C-O-C stretching peaks at 1163 cm^{-1} remain almost insensitive, indicating the epoxy groups can't be eliminated by the reduction process. These results agree well with the Raman spectra, and demonstrate the GO was reduced to the rGO.

Fig. 1C shows the optical photograph of the rGO solution, which has been kept at room temperature for two months. It exhibits that the rGO can be homogeneously dispersed in water. The morphology and microstructure of rGO are shown in Fig. 1D and Fig. 1E, respectively. For the SEM image, translucent rGO sheets with an average size of about 10 μm can be clearly seen. The

specimens are multi-layer graphene and uniformly dispersed due to the electrostatic repulsion force of residual groups on the sheets [20, 31]. Additionally, the TEM image of the rGO shows a layer and wrinkled structure with the thickness of 5 nm, which is in accordance with the SEM image and illuminates the as-prepared rGO are high-quality.

Fig. 2A shows the representative room-temperature engineering stress-strain curves of the unreinforced Ni matrix and graphene/Ni composites prepared by adding different volume of rGO dispersion. It can be observed that the ultimate tensile stress of the graphene/Ni composites is larger than that of the pure Ni. With the rGO dispersions increase from 1 mL to 2 mL, the strength and plasticity of the samples are improving. The highest ultimate tensile strength and fracture elongation obtained are 864 MPa and 20.6 %, the increments compared with the pure Ni being 25 % and 36 % (the tensile strength and elongation rate of the Ni are 690 MPa and 15.1 %), respectively. When the contents of graphene exceed 2 mL, the composites present a decreasing trend in mechanical properties, especially the loss of ductility. The tensile strength of the composite with 5 mL rGO is about 14.7 % greater than that of the Ni, but the fracture elongation is only 7.5 %. The loss of enhancement efficiency in graphene/Ni composites can be explained by the change of microstructures and the agglomeration of graphene [4,32,33]. Fig. 2B summaries the strength and ductility of the previously reported Ni matrix composites reinforced by other reinforcements, such as Gr, CNT, SiC, as well as

the coarse-grained, biomodal, ultrafine, and nanocrystalline nanostructured nickel materials [34-40]. It demonstrates the as-fabricated graphene/Ni composite outperforms most of nickel matrix materials in terms of evading the strength-ductility trade-off.

To study the strengthening mechanism of the graphene/Ni composites with different contents of rGO, the components and microstructures of the samples are investigated. Fig. 3 presents the XRD patterns of Ni and graphene/Ni composites. Two diffraction peaks located at 44.4 ° and 51.8 ° are corresponded to the two crystalline planes of (111) and (200) for the face centred cubic Ni, respectively [41]. The intensity of Ni (111) peak is stronger than that of the Ni (200) peak, but no peaks of graphene are detected. In comparison with the pure Ni, the intensity of Ni (111) peaks for the graphene/Ni composites are similarity, but the Ni (200) peaks present a weak growth trend with the rGO contents increasing. This is quite different from the growth texture reported by Kuang et al. [17], from which the graphene can change the preferred orientation of Ni matrix. Because the addition of rGO can’t obviously change the crystal orientations, the texture is excluded from the main factors that exert considerable influences on the mechanical properties of the graphene/Ni composites.

Fig. 4 shows the grain features of the pure Ni and graphene/Ni composites with 2 mL and 4 mL rGO additives, respectively. According to the EBSD images, it can be clearly seen that all the materials do not have displayed remarkable preferred

orientation of Ni matrix crystal, which is corresponded well with the XRD patterns. However, the grain characteristic, including the geometrical shape, the grain size, and the grain size distribution, are noticeably affected by the rGO. As shown in Fig. 4A, the pure Ni accompanied with a spot of growth twins (account for the total number of 18.5 %) shows a long strip shaped microstructure, for which the average is 0.9 μm, (See Supplementary Figure S1). This makes the pure Ni specimen achieving good tensile elongation. In contrast, the graphene/Ni composite fabricated by adding 2 mL rGO dispersion (in Fig. 4B) possesses a refined grains microstructure, which exhibits a tendency to transform into a bimodal grain size distribution microstructure with ultrafine grain embedded in coarse grain (See Supplementary Figure S2). The bimodal microstructure is caused by the growth inhibition of Ni grains surrounding the homogeneous distributed graphene, and it can significantly enhance the tensile ductility and strength of Ni matrix [15,42,43]. When the contents of rGO increased to 4 mL, the Ni crystals grow into uniformly spherical shape with an average size of 0.7 μm (See Supplementary Figure S3). Owing to the strain localization and a lack of stable deformation, the fine-grained microstructure will bring about the correlation between fatigue limit and yielding strength. According to Fig. 4, it can be seen that these microstructure characteristics are well in accord with the mechanical properties, implying that the strengthening effect of the graphene/Ni composite is closely related to the grain structures.

As reported in previous literatures, the strength improvement of metal matrix composites reinforced by graphene could be attributed to the grain-size refinement strengthen, the Orowan strengthen, the load transfer effects as well as the thermal expansion mismatch [2,4,44]. Among these strengthen mechanisms, the Orowan strengthening and load transfer effects are most important, while the grain-size refinement strengthening also contributes to the tensile strength in the graphene/metal composites. Because of the strong coupling between open d-orbitals, the interface bonding between Ni matrix and graphene reinforcement is strong [45]. Good interface bonding lead to efficient load transfer, accordingly the tensile strength of the graphene/Ni composite can be improved. Furthermore, the strong interfacial bonding also can effectively hinder the crack propagation and final fracture of the composite, and thus induce remarkable toughening on the metal matrix. Unfortunately, the graphene contents of the as-fabricated composites are too low to achieve effective load transfer and prevent the crack propagation (in Table 1). Herein, the high strength and good ductility of the graphene/Ni composites are attributed to the heterogeneous microstructure features. The high strength is obtained with the assistance of high back stress developed from heterogeneous yielding, whereas the high ductility is ascribed to back-stress hardening and dislocation hardening [46].

Since the mechanical properties of the electrodeposited graphene/Ni composites relate to the tuning microstructures, it is interesting to reveal the effects of the

dispersible rGO on the formation of depositions. As shown in Fig. 5, the electrochemical behaviours of the electroplating baths are investigated by the CV and EIS techniques, respectively. It can be seen that a drastic increase in current intensity is appeared at the potential of -650 mV during the cathodic process (in Fig. 5A). The onset potential is corresponding to the deposition potential of Ni cations in electrolyte and represents the nucleation and growth of Ni particles on stainless steel substrates. With the deposition potentials decrease from -650 mV to -1500 mV, the slopes of the CV curves are raising after the addition of rGO dispersion in electroplating baths. This demonstrates that the rGO nanoflakes can promote the cathode polarization effect, consequently augment the deposition rate of Ni matrix. Meanwhile, some oxidation peaks represent at the potential range from -180 mV to -220 mV on the anodic polarization curves. These peaks are associated with the dissolution of the deposited Ni nanocrystallines [47], thus induce the formation of coarse grains. Otherwise, both the potential and current density of the oxidation reaction peak in the CV curve of pure Ni are a little higher than those of the graphene/Ni composites. It indicates the dissolution of Ni nanocrystallines in electroplating bath for pure Ni is much easier than that of the rGO. Herein, the absorption of graphene on electrode not only can increase the cathode polarization effect, but also inhibit the dissolution of nucleating Ni nanocrystallines, accordingly comes to the fine crystalline structures.

Fig. 5B illustrates the Nyquist plots of the pure Ni and graphene/Ni composites. It can be seen that all of the Nyquist plots are similar in shapes with a singular semicircle. Compared with the graphene/Ni composites, the pure Ni exhibits the biggest semi-circular radius. That is to say, the conductivities of the electrodes are improved by the addition of rGO dispersions [48]. Furthermore, the semi-circular radius of graphene/Ni composites with 4 mL and 5 mL rGO are larger than that of the 2 mL and 3 mL, implying a larger resistance in the high rGO contained plating baths. The inset of Fig. 5B displays a selected electrochemical equivalent circuit model, and the calculated values of the electrical circuit parameters are shown in Table 2. In the circuit, R_e is the solution resistance, R_{ct} and Q represent the charge transfer resistance at electrolyte interface and the double layer capacitor, respectively, while Z_w is characterized as the Warburg resistance [49,50]. Even though a small amount of rGO dispersion is added into the plating baths, the R_e and R_{ct} values of the samples are remarkably decreased, especially the R_{ct} value has declined from 359 $k\Omega \cdot cm^{-2}$ to 11.9 $k\Omega \cdot cm^{-2}$. The magnitude decrease in R_{ct} value of composites reveals that the reduction reaction of Ni^{2+} can rapidly occur due to the fast transport of ions and electrons on electrodes, thus bring out the formation of fine grains. These results are consistent with the CV curves, in which the dispersed rGO can promote the electrochemical polarization effect on cathodes. However, as the rGO volume is a little higher in baths (exceed 4 mL), both the R_e and R_{ct} values show a tendency of increasing. This is attributed to the

agglomeration of rGO nanoflakes, for which only a few rGO sheets can adhere to the cathode. The low adsorption quantity of rGO cause a poorer conductive and a slower ion/electron transport rate of the electrodes. Accordingly, the bigger size of metal nickel grains is intended to be formed.

In order to interpret the effects of rGO nanoflakes on the microstructures of the graphene/Ni composites, a possible formation mechanism is proposed in Fig. 6. During the electrodeposition process, both the Ni^{2+} and rGO nanoflakes diffuse and adhere onto the stainless steel substrate, where Ni ions can capture electrons and generate Ni atoms. The absorbed Ni atoms will diffuse along the lateral surface of the cathode, then move to the proper nucleation sites of crystal lattice or meet with other particles. Consequently, the growth of metal matrix brings the co-deposition of Ni and graphene. For the deposition of pure Ni foil, the cathode polarization effect is relatively small, but the dissolution of Ni nanocrystallines on the electrode is serious. The low over-potential will lead a quick crystal growth process, and finally forming a coarse-grained microstructure. In contrast, the rGO nanoflakes play two different roles in the nucleation and growth of the graphene/Ni composites. First, when a low volume rGO dispersion (below 4 mL) has been added into the electroplating bath, the rGO nanoflakes can stably stay in the electrolyte, and randomly absorb on the electrodes under the mechanical stirring force. The homogeneously distributed rGO nanosheets not only can promote the cathodic polarized potential and speed up the transport of

ions/electrons in electrodes, but also provide a large number of nucleation sites. The nucleation rate of Ni crystal is faster than the growth rate in the surrounding area of graphene, where ultrafine grains are formed. Since the larger size grains deposit in the places away from graphene, the as-fabricated composite presents a bimodal microstructure with ultrafine grains embedded in coarse grains. Second, the rGO nanoflakes will agglomerate together in a higher volume bath due to the electrostatic interaction among graphene sheets. Under the circumstances, only a few rGO agglomerations can be incorporated into the Ni matrix, the positive roles of the rGO can't be fully played in the composites. The low cathode polarization effect, poor conductive, as well as the reduction of active sites will make a fine-grained microstructure with uniform size distribution. Hence, by adjusting the added volume of rGO dispersion, it is enable to effectively fabricate graphene/Ni composites with different microstructures and mechanical properties.

Conclusion

The pure Ni foil and graphene/Ni composites have been prepared by adding different volume of dispersive rGO nanofalkes in a direct current deposition process. Compared to the tensile strength and plastic elongation of 690 MPa and 15.1 % for pure Ni, respectively, the graphene/Ni composite with 2 mL rGO demonstrates a high strength of 864 MPa and a good elongation of 20.6 %. The increments in strength and elongation are 25 % and 36 %, respectively. However,

the composite with 5 mL rGO exhibits a strength of 750 MPa, which is 14.7 % greater than that of pure Ni; but the fracture elongation is only 7.5 %. Since the graphene contents in the graphene/Ni composites are too low to achieve effective load transfer and prevent the crack propagation, the enhanced mechanical properties of the composites are related to the heterogeneous microstructure features. A low volume fraction of graphene can promote the cathodic polarized potential, facilitate the transport of ions and electrons on electrodes, as well as provide a large number of nucleation sites, consequently accelerate the formation of bimodal microstructure. In contrast, the agglomeration of rGO sheets in a high-volume plating bath will weak the positive role of rGO in electro-crystallization process. The low adsorption quantity of rGO is unfavourable for the nucleation of Ni matrix, accordingly produces a uniform fine-grained microstructure. These are quite different from the previously reported graphene/Ni composites, in which the graphene reinforcements not only inhibited the growth of grains, but also prevented the propagation of dislocations across the graphene/Ni interfaces. The results suggest that a proper addition of dispersive rGO sheets is propitious to microstructure control of graphene/metal deposits with high strength and good ductility.

Acknowledgements

This work was supported by the National Natural Science Foundation of China (Grant No. 51505318, 51371123), the Natural Science Foundation of Shanxi Province (No. 201601D202033, 201601D202034) and the Innovation Project of Shanxi Graduate Education (No. 2016JD20). The authors are grateful for professor Chengmeng Chen in the Institute of Coal Chemistry, Chinese Academy of Sciences provides the graphene oxide dispersion for experiments.

Supplementary data

Supplementary information: the grain sizes distribution of the grapheme/Ni composites.

References

[1] K.S. Novoselov, V.I. Fal'ko, L. Colombo, P.R. Gellert, M.G. Schwab, K. Kim, A roadmap for graphene, Nature 490 (2012) 192-200.

[2] M.A. Xavior, H.G.P. Kumar, Processing and Characterization Techniques of Graphene Reinforced Metal Matrix Composites (GRMMC): A Review, Mater. Today 4 (2017) 3334-3341.

[3] J.M. Ju, G.F. Wang, K.H. Sim, Facile synthesis of graphene reinforced Al matrix composites with improved dispersion of graphene and enhanced mechanical properties, J. Alloy. Compd. 704 (2017) 585-592.

[4] Z. Hu, G. Tong, D. Lin, C. Chen, H. Guo, J. Xu, L. Zhou, Graphene-reinforced metal matrix nanocomposites - a review, Mater. Sci. Tech-Lond. 32 (2016) 1-24.

[5] K. Fu, X. Zhang, C.S. Shi, E.Z. Liu, F. He, J.J. Li, N.Q. Zhao, C.N. He, An approach for fabricating Ni@graphene reinforced nickel matrix composites with enhanced mechanical properties, Mater. Sci. Eng. A 715 (2018) 108-116.

[6] H.Y. Yue, L.H. Yao, X. Gao, S.L. Zhang, E.J. Guo, H. Zhang, X.Y. Lin, B. Wang, Effect of ball-milling and graphene contents on the mechanical properties and fracture mechanisms of graphene nanosheets reinforced copper matrix composites, J. Alloy. Compd. 691 (2017) 755-762.

[7] X. Du, W.B. Du, Z.H. Wang, K. Liu, S.B. Li, Ultra-high strengthening efficiency of graphene nanoplatelets reinforced magnesium matrix composites, Mater. Sci. Eng. A 711 (2018) 633-642.

[8] T. Cygan, J. Wozniak, M. Kostecki, M. Petrus, A. Jastrzębska, W. Ziemkowska, A. Olszyna, Mechanical properties of graphene oxide reinforced alumina matrix composites, Ceram. Int. 43 (2017) 6180-6186.

[9] R.J. Young, I.A. Kinloch, L. Gong, K.S. Novoselov, The mechanics of graphene nanocomposites: a review, Compos. Sci. Technol. 72 (2012) 1459-1476.

[10] Q.H. Yuan, G.H. Zhou, L. Liao, Y. Liu, L. Luo, Interfacial structure in AZ91 alloy composites reinforced by graphene nanosheets, Carbon 127 (2018) 177-186.

[11] K. Chu, F. Wang, X.H. Wang, Y.B. Li, Z.R. Geng, D.J. Huang, H. Zhang, Interface design of graphene/copper composites by matrix alloying with titanium, Mater. Design 144 (2018) 290-303.

[12] Y.H. Ahmad, A.M.A. Mohamed, Electrodeposition of nanostructured nickel-ceramic composite coatings: a review, Int. J. Electrochem. Sc. 9 (2014) 1942-1963.

[13] L. Lu, Y.F. Shen, X.H. Chen, L.H. Qian, K. Lu, Ultrahigh strength and high electrical conductivity in copper, Science 304 (2004) 422-426.

[14] L.P. Wang, Y. Gao, Q.J. Xue, H.W. Liu, T. Xu, A novel electrodeposited Ni-P gradient deposit for replacement of conventional hard chromium, Surf. Coat. Tech. 200 (2006) 3719-3726.

[15] Q. Zhang, Y. Liu, Y.S. Liu, Y.H. Ren, Y.X. Wu, Z.P. Gao, X.L. Wu, P.D. Han, Enhanced tensile ductility and strength of electrodeposited ultrafine-grained nickel with a desired bimodal microstructure, Mater. Sci. Eng. A 701 (2017) 196-202.

[16] X.X. Shen, J.S. Lian, Z.H. Jiang, Q. Jiang, High strength and high ductility of electrodeposited nanocrystalline Ni with a broad grain size distribution, Mater. Sci. Eng. A 487 (2008) 410-416.

[17] D. Kuang, L.Y. Xu, L. Liu, W.B. Hu, Y.T. Wu, Graphene-nickel composites, Appl. Surf. Sci. 273 (2013) 484-490.

[18] J.H. Li, Z.L. An, Z.Q. Wang, M. Toda, T. Ono, Pulse-reverse electrodeposition and micromachining of graphene-nickel composite: an efficient strategy toward high-performance microsystem application, ACS Appl. Mater. Inter. 8 (2016) 3969-3976.

[19] G.I. Titelman, V. Gelman, S. Bron, R.L. Khalfin, Y. Cohen, H. Bianco-Peled, Characteristics and microstructure of aqueous colloidal dispersions of graphite oxide, Carbon 43 (2005) 641-649.

[20] D. Li, M.B. Müller, S. Gilje, R.B. Kaner, G.G. Wallace, Processable aqueous dispersions of graphene nanosheets, Nat. Nanotechnol. 3 (2008) 101-105.

[21] R. Casati, M. Vedani, Metal matrix composites reinforced by nano-particles - a review, Metals 4 (2014) 65-83.

[22] Z.D. Ren, N. Meng, K. Shehzad, Y. Xu, S.X. Qu, B. Yu, J.K. Luo, Mechanical properties of nickel-graphene composites synthesized by electrochemical deposition, Nanotechnology 26 (2015) 065706.

[23] Y. Li, G.F. Wang, S.Y. Liu, S.S. Zhao, K.F. Zhang, The preparation of Ni/GO composite foils and the enhancement effects of GO in mechanical properties, Compos. Part B-Eng. 135 (2018) 43-48.

[24] C.L. Pavithra, B.V. Sarada, K.V. Rajulapati, T.N. Rao, G. Sundararajan, A new electrochemical approach for the synthesis of copper-Graphene nanocomposite foils with high hardness, Sci. Rep.-UK 4 (2014) 4049.

[25] Y. Li, G.F. Wang, Q. Liu, M. Yang, Ni/GO nanocomposites and its plasticity, Manuf. Rev. 2 (2015) 1-5.

[26] A.C. Ferrari, D.M. Basko, Raman spectroscopy as a versatile tool for studying the properties of graphene, Nat. Nanotechnol. 8 (2013) 235-246.

[27] J.F. Rodriguez-Nieva, E.B. Barros, R. Saito, M.S. Dresselhaus, Disorder-induced double resonant Raman process in graphene, Phys. Rev. B 2014 90.

[28] H.L. Guo, X.F. Wang, Q.Y. Qian, F.B. Wang, X.H. Xia, A green approach to the synthesis of graphene nanosheets, ACS Nano 9 (2009) 2653-2659.

[29] Q. Hu, X. Wang, H. Chen, Z. Wang, Synthesis of Ni/graphene sheets by an electroless Ni-plating method, New Carbon Mater. 27 (2012) 35-41.

[30] N. Li, M. Cao, Q. Wu, C. Hu, A facile one-step method to produce Ni/graphene nanocomposites and their application to the thermal decomposition of ammonium perchlorate, CrystEngComm 14 (2012) 428-434.

[31] Y. Liu, D. Yan, R.F. Zhuo, S.K. Li, Z.G. Wu, J. Wang, P.Y. Ren, P.X. Yan, Z.R. Geng, Design, hydrothermal synthesis and electrochemical properties of porous birnessite-type manganese dioxide nanosheets on graphene as a hybrid material for supercapacitors, J. Power Sources 242 (2013) 78-85.

[32] Z.R. Hu, G.Q. Tong, D. Lin, Q. Nian, J.Y. Shao, Y.W. Hu, M. Saei, S.Y. Jin, G.J. Cheng, Laser sintered graphene nickel nanocomposites, J. Mater. Process. Tech. 231 (2016) 143-150.

[33] C. Zhao, Enhanced strength in reduced graphene oxide/nickel composites prepared by molecular-level mixing for structural applications, Appl. Phys. A 118 (2015) 409-416.

[34] T. Borkar, H. Mohseni, J. Hwang, T.W. Scharf, J. Tiley, S.H. Hong, R. Banerjee, Excellent strengtheductility combination in nickel-graphite nanoplatelet (GNP/Ni) nanocomposites, J. Alloy. Compd. 646 (2015) 135-144.

[35] T. Borkar, J. Hwang, J.Y. Hwang, T.W. Scharf, J. Tiley, S.H. Hong, R. Banerjee, Strength versus ductility in carbon nanotube reinforced nickel matrix nanocomposites, J. Mater. Res. 29 (2014) 761-769.

[36] A.F. Zimmerman, G. Palumbo, K.T. Aust, U. Erb, Mechanical properties of nickel silicon carbide nanocomposites, Mater. Sci. Eng. A 328 (2012) 137-146.

[37] C.D. Gu, J.S. Lian, Q. Jiang, Layered nanostructured Ni with modulated hardness fabricated by surfactant-assistant electrodeposition, Scripta Mater. 57 (2007) 233-236.

[38] Y.M. Wang, S. Cheng, Q.M. Wei, E. Ma, T.G. Nieh, A. Hamza, Effects of annealing and impurities on tensile properties of electrodeposited nanocrystalline Ni, Scripta Mater. 51 (2004) 1023-1028.

[39] X.L. Wu, F.P. Yuan, M.X. Yang, P. Jiang, C.X. Zhang, L. Chen, Y.G. Wei, E. Ma, Nanodomained nickel unite nanocrystal strength with coarse-grain ductility, Sci. Rep.-UK 5 (2015) 11728.

[40] H.W. Yang, F.A. Mohamed, Strength and ductility in electrodeposited nanocrystalline nickel, Mate. Sci. Forum 633 (2010) 411-420.

[41] K. Jiang, J. Li, J. Liu, Electrochemical codeposition of graphene platelets and nickel for improved corrosion resistant properties, RSC Adv. 4 (2014) 36245.

[42] Y.H. Zhao, T. Topping, J.F. Bingert, J.J. Thornton, A.M. Dangelewicz, Y. Li, W. Liu, Y.T. Zhu, Y.Z. Zhou, E.J. Lavernia, High tensile ductility and strength in bulk nanostructured nickel, Adv. Mater. 20 (2008) 3028-3033.

[43] C.D. Gu, J.S. Lian, Z.H. Jiang, Q. Jiang, Enhanced tensile ductility in an electrodeposited nanocrystalline Ni, Scripta Mater. 54 (2006) 579-584.

[44] X. Zhang, C.S. Shi, E.Z. Liu, F. He, L.Y. Ma, Q.Y. Li, J.J. Li, W. Bacs, N.Q. Zhao, C.N. He, Achieving high strength and high ductility in metal matrix composites reinforced with a discontinuous three-dimensional graphene-like network, Nanoscale 9 (2017) 11929-11938.

[45] V.N. Do, H.A. Le, Transport characteristics of graphene-metal interfaces, Applied Phys. Lett. A 101 (2012) 161-165.

[46] X.L. Wu, M.X. Yang, F.P Yuan, G.L Wu, Y.J Wei, X.X Huang, Y.T. Zhu, Heterogeneous lamella structure unites ultrafine-grain strength with coarse-grain ductility, P. Natl. Acad. Sci. USA 112 (2015) 14501-14505.

[47] R. Mishra, R. Balasubramaniam, Effect of nanocrystalline grain size on the electrochemical and corrosion behavior of nickel, Corros. Sci. 46 (2004) 3019-3029.

[48] Y. Wang, K. Huang, A. Derré, P. Puech, S. Rouzière, P. Launois, C. Castro, M. Monthioux, A. Pénicaud, Conductive graphene coatings synthesized from graphenide solutions, Carbon 121 (2017) 217-225.

[49] Y. Zhou, F. Q. Xie, X. Q. Wu, W. D. Zhao, X. Chen, A novel plating apparatus for electrodeposition of Ni-SiC composite coatings using circulating-solution co-deposition technique, J. Alloy. Compd. 699 (2017) 366-377.

[50] M.D. Stoller, S. Park, Y.W. Zhu, J.H. An, R.S. Ruoff, Graphene-based ultracapacitors, Nano Lett. 10 (2008) 3498-3502.

Fig.1 The microstructures and morphologies of the as-synthesized GO and rGO, respectively. (A) Raman Spectra, (B) FT-IR spectra, (C) Optical images after two months of preparation, (D) SEM images, (E) TEM images of rGO.

Fig.2 Tensile stress-strain curves of graphene/Ni composites. (A) Engineering stress-strain curves of the pure Ni and graphene/Ni composites, (B) Yield strength versus the total tensile elongation of Ni in comparison with available literature data.

Fig.3 XRD patterns of the pure Ni and graphene/Ni composites.

Fig.4 EBSD mapping of the pure Ni and graphene/Ni composites. (A) Ni, (B) The graphene/Ni composites with 2 mL rGO dispersions, (C) The graphene/Ni composites with 4 mL rGO dispersions, (D) The color map of crystallographic orientation.

Fig.5 The electrochemical behaviors of the pure Ni and graphene/Ni composites. (A) Cyclic voltammogram, (B) Nyquist plots, and the inset is the equivalent electrical circuit.

Fig.6 Schematic illustration of the formation mechanism of the graphene/Ni composites with different rGO content.

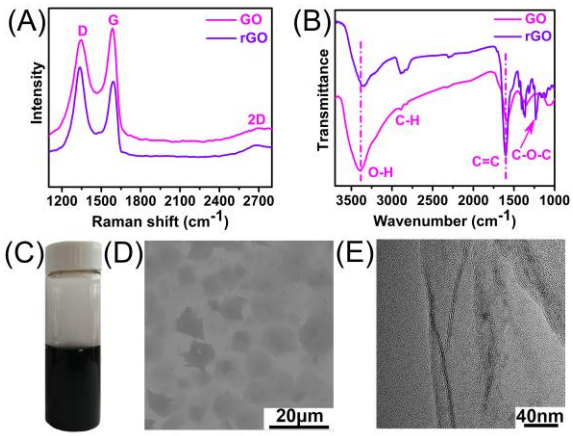

Fig. 1

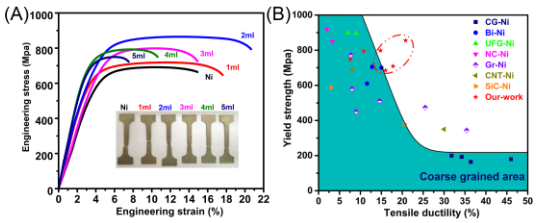

Fig. 2

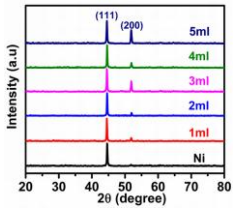

Fig. 3

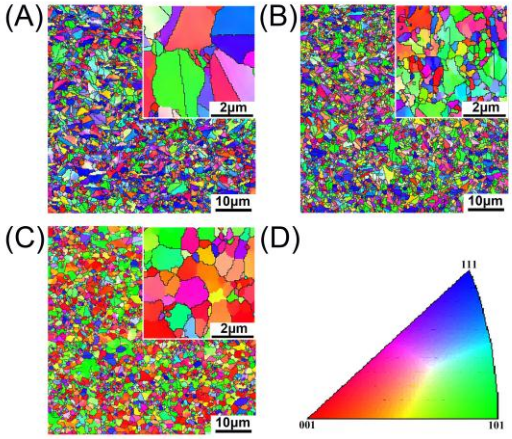

Fig. 4

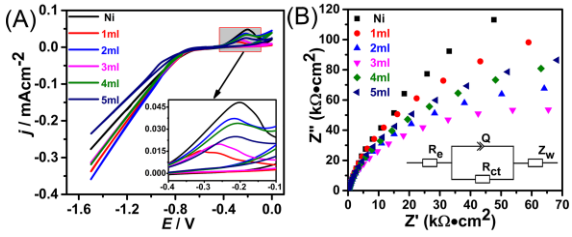

Fig. 5

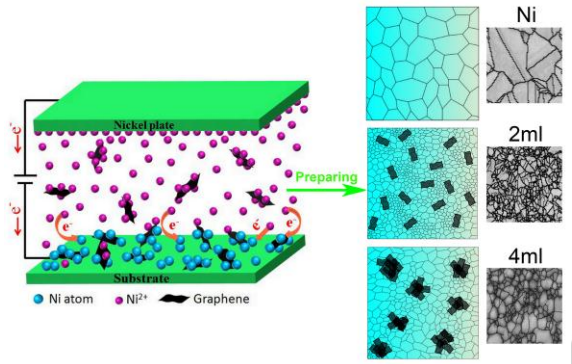

Fig. 6

Table.1 The chemical composition of graphene/Ni composite specimens.

Materials	C (wt%)	Ni (wt%)
Ni	0.001	99.999
2mL	0.008	99.992
4mL	0.014	99.986

Table.2 Fitting results of impedance spectra of the as-synthesized graphene/Ni composites.

Materials	R_e ($\Omega \cdot cm^2$)	Q ($\mu F \cdot cm^{-2}$)	n	R_{ct} ($k\Omega \cdot cm^{-2}$)	Z_W ($\Omega \cdot cm^2 s^{-1/2}$)	Error (%)
Ni	77.99	1.04×10^{-4}	0.9436	359	2.07×10^{-3}	0.511
1 mL	77.00	1.00×10^{-4}	0.9337	26.8	3.17×10^{-2}	1.149
2 mL	64.17	1.03×10^{-4}	0.9289	15.2	3.27×10^{-3}	1.367
3 mL	59.73	9.93×10^{-5}	0.9272	11.9	3.42×10^{-3}	0.953
4 mL	77.46	9.10×10^{-5}	0.9162	20.3	1.17×10^{-2}	1.514
5 mL	95.26	9.67×10^{-5}	0.9114	21.3	1.05×10^{-2}	1.450